Immunogenomic identification and characterization of granulocytic myeloid derived suppressor cells in multiple myeloma

Authors: Cristina Perez [1*], Cirino Botta [1,2*], Aintzane Zabaleta [1], Noemi Puig [3], Maria-Teresa Cedena [4], Ibai Goicoechea [1], Daniel Alameda [1], Edurne San José-Eneriz[1], Juana Merino [1], Paula Rodriguez-Otero [1], Catarina Maia [1], Diego Alignani [1], Patricia Maiso [1], Irene Manrique [1], David Lara-Astiaso [1], Amaia Vilas-Zornoza [1], Sarai Sarvide [1], Caterina Riillo [5], Marco Rossi [5], Laura Rosiñol [6], Albert Oriol [7], María-Jesús Blanchard [8], Rafael Rios [9], Anna Sureda [10], Jesus Martin [11], Rafael Martinez [12], Joan Bargay [13], Javier de la Rubia [14,15], Miguel-Teodoro Hernandez [16], Joaquin Martinez-Lopez [4], Alberto Orfao [17], Xabier Agirre [1], Felipe Prosper [1], Maria-Victoria Mateos [3], Juan-José Lahuerta [4], Joan Blade [6], Jesús F. San-Miguel [1], Bruno Paiva [1], on behalf of the GEM (Grupo Español de Mieloma)/PETHEMA (Programa para el Estudio de la Terapéutica en Hemopatías Malignas) cooperative study group.

* Have contributed equally to this study and should be considered as first authors.

Affiliations: 1) Clinica Universidad de Navarra, Centro de Investigacion Medica Aplicada (CIMA), Instituto de Investigacion Sanitaria de Navarra (IDISNA), CIBER-ONC numbers CB16/12/00369, CB16/12/00489, Pamplona, Spain; 2) Department of Oncohematology, “Annunziata” Hospital, Cosenza, Italy; 3) Hospital Universitario de Salamanca, Instituto de Investigacion Biomedica de Salamanca (IBSAL), Centro de Investigación del Cancer (IBMCC-USAL, CSIC), CIBER-ONC number CB16/12/00233 Salamanca, Spain; 4) Hospital 12 de Octubre, CIBER-ONC number CB16/12/00369, Madrid, Spain; 5) Department of Clinical and Experimental Medicine, “Magna Graecia” University of Catanzaro, Italy; 6) Hospital Clínic IDIBAPS, Barcelona, Spain; 7) Institut Català d’Oncologia i Institut Josep Carreras, Badalona, Spain; 8) Hospital Ramón y Cajal, Madrid, Spain; 9) Hospital Virgen de las Nieves, Granada, Spain; 10) Institut Català d’Oncologia-Hospitalet, IDIBELL, Barcelona. 11) Hospital Universitario Virgen del Rocío, Instituto de Biomedicina de Sevilla (IBIS/CSIC/CIBERONC CB16/12/00480); 12) Hospital Clínico San Carlos, Madrid; 13) Hospital Son Llatzer, Palma de Mallorca; 14) Hospital Universitario y Politécnico La Fe, Valencia; 15) School of Medicine and Dentistry, Catholic University of Valencia, Valencia; 16) Hospital Universitario de Canarias, Santa Cruz de Tenerife; 17) Cancer Research Center (IBMCC-CSIC/USAL-IBSAL); Cytometry Service (NUCLEUS) and Department of Medicine, University of Salamanca, Salamanca, Spain (USAL). Centro de Investigación Biomédica en Red de Cáncer, Instituto Carlos III, Madrid, Spain. CIBER-ONC number CB16/12/00400. Spain

Address for correspondence:

Bruno Paiva, Ph.D.

Clínica Universidad de Navarra; Centro de Investigación Médica Aplicada (CIMA)

Av. Pío XII 55, 31008 Pamplona, Spain

e-mail: bpaiva@unav.es

Hospital	Investigator
Complejo Hospitalario Costa del Sol	Dra. María Casanova Espinosa
H. Especialidades de Jerez de la Frontera	Dr. José Luís Guzman Zamudio
H. Nuestra Señora de Valme	Dr. Eduardo Ríos Herranz
H. Universitario Virgen de las Nieves	Dr. Rafael Rios Tamayo
Complejo Hospitalario Regional Virgen del Rocío	Dr. Jesús Martín Sánchez
H. Clínico Universitario Lozano Blesa	Dr. Luís Palomera Bernal
H. Universitario Central de Asturias	Dra. Ana Pilar González Rodríguez
H. Cabueñes	Dra. María Esther González García
Complejo Asistencial Son Espases	Dra. Antonia Sampol Mayol
H. Son Llátzer	Dr. Joan Bargay Lleonart
H. de Gran Canaria Dr. Negrín	Dra. Alexia Suárez
H. Universitario de Canarias	Dr. Miguel Teodoro Hernández García
H. Universitario Marqués de Valdecilla	Dra. Carmen Montes Gaisán
H. General de Ciudad Real	Dra. Belén Hernández Ruiz
Complejo Hospitalario de Toledo	Dr. Felipe Casado Montero
H. Universitario de Guadalajara	Dra. Dunia de Miguel Llorente
H. Nuestra Señora del Prado (Talavera)	Dr. Fernando Solano Ramos
H. General de Albacete	Dra. Ángela Ibañez Garcia
H. Clínico de Salamanca	Dra. Mariví Mateos Manteca
Complejo Hospitalario H. General de Segovia	Dr. José Mariano Hernández Martín

H. de León	Dr. Fernando Escalante Barrigón
H. Universitario Rio Hortega	Dr. Javier García Frade
H. Clínico Universitario de Valladolid	Dr. Alfonso García de Coca
H. Santa Bárbara	Dr. Carlos Aguilar Franco
Hospital Universitario de Burgos	Dr. Jorge Labrador Gómez:
H. Althaia, Xarxa Asistencial de Manresa (Sant Joan de Deu)	Dra. Elena Cabezudo Pérez
H CLINIC	Dr. Joan Bladé Creixentí
H. Durán i Reynals - ICO L´Hospitalet	Dra. Ana Mª Sureda Balari
ICO Girona, H. Universitario de Girona Dr. Josep Trueta	Dra. Yolanda González Montes
H. UNIVERSITARI JOAN XXII DE TARRAGONA	Dra. Lourdes Escoda Teigell
Hospital Universitari Arnau de Vilanova de Lleida	Dr. Antonio García Guiñón
H. del Mar	Dra. Eugenia Abella Monreal
H. de Sabadell (Parc Taulí)	Dr. Juan Alfonso Soler Campos
Hospital Universitario Mútua de Terrassa	Dr. Josep Mª Martí Tutusaus
H. Germans Trias i Pujol	Dr. Albert Oriol Rocafiguera
H. de la Santa Creu i Sant Pau	Dr. Miquel Granell Gorrochategui
H. Vall d´Hebrón	Dra. Mercedes Gironella Mesa
H. San Pedro de Alcántara (Complejo Hospitalario de Cáceres)	Dra. Carmen Cabrera Silva
Complejo Hospitalario Universitario de Santiago	Dra. Marta Sonia González Pérez
Complejo Hospitalario de Pontevedra	Dra. Ana Dios Loureiro
Complejo Hospitalario de Ourense	José Angel Méndez Sánchez
H. San Pedro	Dra. María Josefa Nájera Irazu
H. Universitario Fundación de Alcorcón	Dr. Francisco Javier Peñalver Párraga
H. Universitario 12 de Octubre	Dr. Juan José Lahuerta Palacios
H. de Fuenlabrada	Dra. Pilar Bravo Barahona
H. General Universitario Gregorio Marañón	Dra. Cristina Encinas Rodríguez
H. Infanta Leonor	Dr. José Ángel Hernández Rivas

H. Universitario Madrid - Sanchinarro	Dr. Jaime Pérez de Oteyza
Centro Oncológico MD Anderson	Dra. Rebeca Iglesias del Barrio
H. Universitario La Paz	Dra. Ana López de la Guia
H. Universitario de la Princesa	Dr. Adrián Alegre Amor
Fundación Jiménez Díaz-UTE	Dra. Elena Prieto Pareja
Hospital Universitario Puerta de Hierro - Majadahonda	Dra. Isabel Krsnik Castelló
H. Ramón y Cajal	Dra. Mª Jesús Blanchard Rodríguez
H. Universitario de San Carlos	Dr. Rafael Martínez Martínez
H. Severo Ochoa	Dra. Rosalía Riaza Grau
H. INFANTA SOFÍA	Dr. Eugenio Giménez Mesa
HOSPITAL DEL TAJO	Dra. Elena Ruiz Sainz
H. Morales Meseguer	Dr. Felipe de Arriba
H. Universitario Virgen de la Arrixaca	Dr. Jose María Moraleda Jiménez
H. General Universitario Santa Lucia	Dra. Marta Romera
Clínica Universidad de Navarra	Dr. Felipe Prósper Cardoso
Complejo Hospitalario de Navarra	Dr. José Mª Arguiñano Pérez
H. de Cruces	Dra. María Puente Pomposo
H. de Txagorritxu	Dr. Ernesto Pérez Persona
H. Clínico Universitario de Valencia	Dra. Ana Isabel Teruel Casasús
H. Universitario Dr. Peset	Dra. Paz Ribas García
H. Universitario La Fe	Dr. Isidro Jarque Ramos
H. General Universitario de Alicante	Dra. María Blanca Villarrubia Lor
H. TORREVIEJA SALUD UTE	Dr. Pedro Luis Fernández García
H. del Vinalopo	Dr. Pedro Luis Fernández García
H. Quirón	Dra. Carmen Martínez Chamorro

TABLE OF CONTENT

SUPPLEMENTAL METHODS

Automated clustering. We used FlowSOM [17] for automated clustering. Briefly, it works following a four-step approach: 1) reading data; 2) building a self-organizing map (SOM) for clustering and dimensionality reduction; 3) building a minimum spanning tree connecting nodes according to their similarity; 4) computing an automated meta-clustering by grouping similar nodes. The meta-clustering step is critical for the definition of cell populations. In this phase, groups of similar nodes are "fused" to obtain more consistent populations following specific algorithms. We used the ConsensusClusterPlus package separated from FlowSOM to obtain better control of each function. At this stage it is possible to decide the final number of clusters in which cells are being divided.

Cytospin. A total of $1x10^6$ cells from various neutrophil subsets were sorted in PBS. Afterwards, cells were attached to slides by cytocentrifugation (Thermo Fisher Scientific, Waltham, MA). Slides were stained following the May-Grünwald/Giemsa method and evaluated in an optical microscope (CX-21; Olympus, Tokyo, Japan). Images are shown with a 400x magnification.

T cell proliferation. The impact in T cell proliferation of various neutrophil subsets was evaluated through FACSorting of each neutrophil subset and autologous T cells from bone marrow (BM) samples of multiple myeloma (MM) patients (N = 10) and healthy adults (HA) (N = 4). T cells were labelled with Violet Proliferation Dye (VPD) 450 (BD Horizon™) according to the manufacturer's protocol. Afterwards, $0.4x10^5$ T cells were seeded per well in a 96-well U bottom plate previously coated with an anti-CD3 monoclonal antibody 2.5 µg/mL (overnight at 4ºC, eBioscience™ San Diego, CA). This process was repeated for each neutrophil subsets, which were cultured with T cells in an E:T ratio of 1:1 in RPMI1640 medium (10% FBS, 1% L-Glu, 1% Penicillin-Streptomycin) and in presence of 1.2 µg/mL of an anti-CD28 monoclonal antibody (eBioscience™ San Diego, CA, USA). After a 4-day incubation at 37ºC, cells were labelled with CD45-OC515, CD15-FITC, CD8-PE, 7AAD-PerCP-Cy5.5, CD4-PE-Cy7 and CD3-APCH7. Data acquisition was performed in a FACSCantoII flow cytometer and T cell proliferation was analyzed using the Infinicyt software, based on the diffusion of VPD to daughter cells.

T cell immunosuppression. We established unique culture conditions to evaluate the immunosuppressive potential of various neutrophil subsets after depleting a single subset in each condition (N = 10). $0.25x10^6$ cells per condition were seeded in a 96-well plate and cultured in presence or absence of 30 nM of a BCMAxCD3 bispecific antibody

in RPMI1640 medium (10% FBS, 1% L-Glu, 1% Penicillin-Streptomycin). After overnight incubation at 37ºC, cells were labelled with CD11b-BV421, CD45-KromeOrange, CD38-FITC, CD229-PE, CD16-PerCP-Cy5.5, CD56-PE-Cy7, Annexin-V-APC and CD138-APCH7. MM cell death was determined according to the percentage of Annexin-V+ cells measured in a FACSCantoII flow cytometer. Data analysis was performed using the Infinicyt software.

RNA sequencing (RNAseq). Various neutrophil subsets were isolated from total BM samples of HA (N = 8) and MM patients (N = 8) in a FACSAriaII. Bulk RNAseq was obtained using a protocol adapted from single-cell massively parallel single-cell RNA-sequencing [18], which enabled preparing libraries with as few as 20,000 cells as starting material. Briefly, we barcoded RNA from each sample in a retrotranscription (RT) reaction with AffinityScript Multiple Temperature Reverse Transcriptase (Agilent, Santa Clara, CA) and different RT primers. After qPCR, cDNA with similar Ct values were pooled together. cDNA was purified with SPRIselect 1.2X (Beckman Coulter –BC-, Brea, CA) and amplified using the T7 promotor as template previously introduced in the RT reaction. T7 polimerase (NEB) was added for 16 hours at 37ºC. RNA molecules were fragmented with 2µL of 10X Zn^{2+} fragmentation buffer (Ambion™, ThermoFisher) for 1 min at 70ºC and purified with SPRIselect 2X. Afterwards, a ssRNA adaptor (Illumina, San Diego, CA) was ligated to the 3'-end of the RNA fragments in presence of DMSO, 100 mM ATP, 50% PEG and T4 RNA ligase I (NEB) for 2 hours at 22ºC. A second RT reaction was performed with AffinityScript Multiple Temperature Reverse Transcriptase and resulting cDNA was purified with SPRIselect 1.5X. Finally, cDNA was amplified with 12.5µL Kappa Hifi ready mix + 1µL 25 µM primer mix per sample and purified with SPRIselect 0.7X. Qubit, TapeStation and qPCR analysis were done as quality controls and 4 nM of the final library were sequenced in a NextSeq (Illumina).

Differential gene expression across all pairwise comparisons between groups was analyzed with Deseq2 R package followed by k-means clustering of genes in R. A one-way ANOVA with multiple comparisons was used to determine the significance of differential gene expression across each neutrophil subset, between neutrophils derived from HA and MM patients, between neutrophils derived from peripheral blood or bone marrow and before and after treatment with hypomethylating agents. Genes with a $P<0.05$ were used for gene ontology analysis and gene set enrichment analysis using the *clusterprofiler* and *fgsea* R packages, respectively.

Treatment with TGF-β. We exposed whole PB from HA (N = 3) to 1ng/mL of TGF-β for 48 hours. After incubation at 37ºC, cells were labelled with SYTOX™ Blue (Thermo

Fisher Scientific, MA, USA), CD15-FITC, CD13-PE, CD45-PerCP-Cy5.5, CD16-PE-Cy7 and CD11b-APC and mature neutrophils were stored in Lysis/Binding Buffer (Invitrogen™, CA, USA) for RNAseq using the protocols described above.

Assay for Transposase Accessible Chromatin with high-throughput sequencing (ATACseq). Approximately 20,000 cells of various neutrophils subsets were FACSorted from total BM samples of HA (N = 3) or MM patients (N = 3), and placed in a PCR tube with 100µL of PBS+BSA 0.05%. After centrifugation (500g, 4ºC, 10 min), the pellet was suspended in 25µL of the transposase reaction mixture (15µL of Buffer TD2x (Illumina), 1µL of TDE1 enzyme (Illumina), 0.25µL of 5% digitonin (Promega) and 8.75µL of nuclease-free water). The resulting mix was incubated at 37ºC for 30 min at 450 rpm. Afterwards, the transposase reaction was stopped on ice and 5µL of clean up buffer, 2µL of 5% SDS and 2µL of Proteinase K (New England Biolabs) were added to the previous mix and incubated for 30 min at 40ºC. Transposase-reaction products were cleaned up with AMPure magnetic beads 2X (BC). Finally, the DNA fragments were amplified with 22µL Kappa Hifi ready mix + 4µL of primer 1 i5 and 2 i7 mix per sample. Library was purified with AMPure magnetic beads 2X. Quality control was performed with Qubit and TapeStation, and 4 nM of the final library were sequenced in a NextSeq.

ATACseq reads were aligned to the hg19 genome build using bowtie2 with default parameters (except commands adapted for these specific data such as --very-sensitive and --non-deterministic options that improve accuracy and results when there are many identical reads) and filtered based on mapping score (MAPQ ≥ 30) by Samtools version 1.3.159. The MACS2 version 2.1.0 was used to identify peaks for each sample with default settings. *ChiPQC* package was used for quality control and blacklisted peaks removal. *ChipSeeker* was used to assess overlap of differential peaks and relate peaks to annotated transcription start sites using default options. DESeq2 was used to normalize and identify differential peaks across treatment conditions with p-value <0.05. *Clusterprofiler* R package was used to perform a gene ontology analysis.

Epigenetic targeting. We treated whole BM samples from MM patients (N = 3) with a selective and reversible inhibitor of histone methyltransferase G9a and DNA-methyltransferase [24] (CM-272), testing two different drug concentrations (250 and 500 nM). Approximately $3x10^6$ cells were seeded per well in a 24-well plate and left in culture for 48 hours. Cells were treated at time 0 and +24 hours. After incubation at 37ºC, cells were labelled with SYTOX™ Blue (Thermo Fisher Scientific, MA, USA), CD15-FITC, CD13-PE, CD45-PerCP-Cy5.5, CD16-PE-Cy7 and CD11b-APC to evaluate the distribution of neutrophil subsets after drug exposure. We also investigated a possible

synergic effect between CM-272 and a BCMAxCD3 bispecific antibody in two functional assays. First, we analyzed the immunosuppressive potential of various neutrophils subsets present in BM samples of MM patients (N = 5) after depleting a single subset with FACS. A total of $0.25x10^6$ cells per condition were seeded in a 96-well plate and pre-incubated for 2-hours with CM-272 (10nM) at 37ºC. After washing to remove the compound, $0.5x10^5$ H929 MM cells were added to the culture followed by incubation with a BCMAxCD3 bispecific antibody (30nM) for 24-hours at 37ºC in RPMI1640 medium (10% FBS, 1% L-Glu, 1% Penicillin-Streptomycin). Secondly, we analyzed the cytotoxic effect of T cells in the presence of each neutrophil subset, sorted from BM samples of MM patients (N = 5). A total of $0.5x10^5$ cells were seeded in a 96-well plate. Neutrophils were preincubated for 2-hours with CM-272 (10nM) at 37ºC. After washing to remove the compound, $0.5x10^5$ H929 MM cells and $0.5x10^5$ T cells were added to the culture and incubated with a BCMAxCD3 bispecific antibody (30nM) for 24-hours at 37ºC in RPMI1640 medium. Cells were labelled with CD11b-BV421, CD45-KromeOrange, CD38-FITC, CD229-PE, CD16-PerCP-Cy5.5, CD56-PE-Cy7, Annexin-V-APC and CD138-APCH7. MM cell death was determined according to the percentage of Annexin-V+ H929 cells measured in a FACSCantoII flow cytometer. Data analysis was performed using the Infinicyt software.

REFERENCES

1. Gabrilovich DI, Ostrand-Rosenberg S, Bronte V. Coordinated regulation of myeloid cells by tumours. *Nat Rev Immunol*. 2012;12(4):253-268.

2. Botta C, Gulla A, Correale P, Tagliaferri P, Tassone P. Myeloid-derived suppressor cells in multiple myeloma: pre-clinical research and translational opportunities. *Front Oncol*. 2014;4:348.

3. Gabrilovich DI, Nagaraj S. Myeloid-derived suppressor cells as regulators of the immune system. *Nat Rev Immunol*. 2009;9(3):162-174.

4. Giese MA, Hind LE, Huttenlocher A. Neutrophil plasticity in the tumor microenvironment. *Blood*. 2019;133(20):2159-2167.

5. Bronte V, Brandau S, Chen SH, et al. Recommendations for myeloid-derived suppressor cell nomenclature and characterization standards. *Nat Commun*. 2016;7:12150.

6. Greten TF, Manns MP, Korangy F. Myeloid derived suppressor cells in human diseases. *Int Immunopharmacol*. 2011;11(7):802-807.

7. De Veirman K, Van Valckenborgh E, Lahmar Q, et al. Myeloid-derived suppressor cells as therapeutic target in hematological malignancies. *Front Oncol*. 2014;4:349.

8. Malek E, de Lima M, Letterio JJ, et al. Myeloid-derived suppressor cells: The green light for myeloma immune escape. *Blood Rev*. 2016;30(5):341-348.

9. Ramachandran IR, Martner A, Pisklakova A, et al. Myeloid-derived suppressor cells regulate growth of multiple myeloma by inhibiting T cells in bone marrow. *J Immunol*. 2013;190(7):3815-3823.

10. Tadmor T. The growing link between multiple myeloma and myeloid derived suppressor cells. *Leuk Lymphoma*. 2014;55(12):2681-2682.

11. Krejcik J, Casneuf T, Nijhof IS, et al. Daratumumab depletes CD38+ immune regulatory cells, promotes T-cell expansion, and skews T-cell repertoire in multiple myeloma. *Blood*. 2016;128(3):384-394.

12. De Veirman K, Menu E, Maes K, et al. Myeloid-derived suppressor cells induce multiple myeloma cell survival by activating the AMPK pathway. *Cancer Lett*. 2019;442:233-241.

13. Wang J, De Veirman K, De Beule N, et al. The bone marrow microenvironment enhances multiple myeloma progression by exosome-mediated activation of myeloid-derived suppressor cells. *Oncotarget*. 2015;6(41):43992-44004.

14. Rosinol L, Oriol A, Rios R, et al. Bortezomib, lenalidomide, and dexamethasone as induction therapy prior to autologous transplant in multiple myeloma. *Blood*. 2019;134(16):1337-1345.

15. Paiva B, Puig N, Cedena MT, et al. Measurable Residual Disease by Next-Generation Flow Cytometry in Multiple Myeloma. *J Clin Oncol*. 2019:JCO1901231.

16. Chesney JA, Mitchell RA, Yaddanapudi K. Myeloid-derived suppressor cells-a new therapeutic target to overcome resistance to cancer immunotherapy. *J Leukoc Biol*. 2017;102(3):727-740.

17. Van Gassen S, Callebaut B, Van Helden MJ, et al. FlowSOM: Using self-organizing maps for visualization and interpretation of cytometry data. *Cytometry A*. 2015;87(7):636-645.

18. Flores-Montero J, Sanoja-Flores L, Paiva B, Puig N, García-Sánchez O, Böttcher S, et al. Next Generation Flow for highly sensitive and standardized detection of minimal residual disease in multiple myeloma. *Leukemia*. 2017;31(10):2094–103.

19. Alameda D, Saez B, Lara-Astiaso D, et al. Characterization of freshly isolated mesenchymal stromal cells from healthy and multiple myeloma bone marrow: transcriptional modulation of the microenvironment. *Haematologica*. 2020.

20. Gorgun GT, Whitehill G, Anderson JL, et al. Tumor-promoting immune-suppressive myeloid-derived suppressor cells in the multiple myeloma microenvironment in humans. *Blood*. 2013;121(15):2975-2987.

21. Frassanito MA, De Veirman K, Desantis V, et al. Halting pro-survival autophagy by TGFbeta inhibition in bone marrow fibroblasts overcomes bortezomib resistance in multiple myeloma patients. *Leukemia*. 2016;30(3):640-648

22. Lu A, Pallero MA, Lei W, et al. Inhibition of Transforming Growth Factor-beta Activation Diminishes Tumor Progression and Osteolytic Bone Disease in Mouse Models of Multiple Myeloma. *Am J Pathol*. 2016;186(3):678-690.

23. Lu A, Pallero MA, Lei W, et al. Inhibition of Transforming Growth Factor-beta Activation Diminishes Tumor Progression and Osteolytic Bone Disease in Mouse Models of Multiple Myeloma. *Am J Pathol*. 2016;186(3):678-690.

24. San Jose-Eneriz E, Agirre X, Rabal O, et al. Discovery of first-in-class reversible dual small molecule inhibitors against G9a and DNMTs in hematological malignancies. *Nat Commun*. 2017;8:15424.

25. Facon T, Kumar S, Plesner T, et al. Daratumumab plus Lenalidomide and Dexamethasone for Untreated Myeloma. *N Engl J Med*. 2019;380(22):2104-2115.

26. Mateos MV, Hernandez MT, Giraldo P, et al. Lenalidomide plus dexamethasone for high-risk smoldering multiple myeloma. *N Engl J Med*. 2013;369(5):438-447.

27. Raje N, Berdeja J, Lin Y, et al. Anti-BCMA CAR T-Cell Therapy bb2121 in Relapsed or Refractory Multiple Myeloma. *N Engl J Med*. 2019;380(18):1726-1737.

28. Gabrilovich DI, Bronte V, Chen SH, et al. The terminology issue for myeloid-derived suppressor cells. *Cancer Res*. 2007;67(1):425; author reply 426.

29. Sagiv JY, Michaeli J, Assi S, et al. Phenotypic diversity and plasticity in circulating neutrophil subpopulations in cancer. *Cell Rep*. 2015;10(4):562-573.

30. Pillay J, Tak T, Kamp VM, Koenderman L. Immune suppression by neutrophils and granulocytic myeloid-derived suppressor cells: similarities and differences. *Cell Mol Life Sci*. 2013;70(20):3813-3827.

31. Damasceno D, Andres MP, van den Bossche WB, et al. Expression profile of novel cell surface molecules on different subsets of human peripheral blood antigen-presenting cells. *Clin Transl Immunology*. 2016;5(9):e100.

32. Condamine T, Mastio J, Gabrilovich DI. Transcriptional regulation of myeloid-derived suppressor cells. *J Leukoc Biol*. 2015;98(6):913-922.

33. Fan C, Stendahl U, Stjernberg N, Beckman L. Association between orosomucoid types and cancer. *Oncology*. 1995;52(6):498-500.

34. Yuan M, Zhu H, Xu J, Zheng Y, Cao X, Liu Q. Tumor-Derived CXCL1 Promotes Lung Cancer Growth via Recruitment of Tumor-Associated Neutrophils. *J Immunol Res*. 2016;2016:6530410.

35. Ng LG, Ostuni R, Hidalgo A. Heterogeneity of neutrophils. *Nat Rev Immunol*. 2019;19(4):255-265.

36. Andzinski L, Kasnitz N, Stahnke S, et al. Type I IFNs induce anti-tumor polarization of tumor associated neutrophils in mice and human. *Int J Cancer*. 2016;138(8):1982-1993.

37. Pylaeva E, Lang S, Jablonska J. The Essential Role of Type I Interferons in Differentiation and Activation of Tumor-Associated Neutrophils. *Front Immunol*. 2016;7:629.

38. Jaitin DA, Keningsberg E, Keren-Shaul H, et al. Massively parallel single-cell RNA-seq for marker-free decomposition of tissues into cell types. *Science*. 2014;343(6172):776-779.

Supplemental Table 1. KEGG cytokine-cytokine receptor interaction pathway list.

AC005840.1	CCR6	EPO	IL12RB1	IL7R	TNFRSF11B
ACVR1	CCR7	EPOR	IL12RB2	IL8	TNFRSF12A
ACVR1B	CCR8	FAS	IL13	IL9	TNFRSF13B
ACVR2A	CCR9	FASLG	IL13RA1	IL9R	TNFRSF13C
ACVR2B	CD27	FLT1	IL15	INHBA	TNFRSF14
ACVRL1	CD40	FLT3	IL15RA	INHBB	TNFRSF17
AMH	CD40LG	FLT3LG	IL17A	INHBC	TNFRSF18
AMHR2	CD70	FLT4	IL17B	INHBE	TNFRSF19
BMP2	CLCF1	GDF5	IL17RA	KDR	TNFRSF1A
BMP7	CNTF	GH1	IL17RB	KIT	TNFRSF1B
BMPR1A	CNTFR	GH2	IL18	KITLG	TNFRSF21
BMPR1B	CRLF2	GHR	IL18R1	LEP	TNFRSF25
BMPR2	CSF1	HGF	IL18RAP	LEPR	TNFRSF4
CCL1	CSF1R	IFNA1	IL19	LIF	TNFRSF6B
CCL11	CSF2	IFNA10	IL1A	LIFR	TNFRSF8
CCL13	CSF2RA	IFNA13	IL1B	LTA	TNFRSF9
CCL14	CSF2RB	IFNA14	IL1R1	LTB	TNFSF10
CCL15	CSF3	IFNA16	IL1R2	MET	TNFSF11
CCL16	CSF3R	IFNA17	IL1RAP	MPL	TNFSF12
CCL17	CTF1	IFNA2	IL2	NGFR	TNFSF13
CCL18	CX3CL1	IFNA21	IL20	OSM	TNFSF13B
CCL19	CX3CR1	IFNA4	IL20RA	OSMR	TNFSF14
CCL2	CXCL1	IFNA5	IL20RB	PDGFA	TNFSF15
CCL20	CXCL10	IFNA6	IL21	PDGFB	TNFSF18
CCL21	CXCL11	IFNA7	IL21R	PDGFC	TNFSF4
CCL22	CXCL12	IFNA8	IL22	PDGFRA	TNFSF8
CCL23	CXCL13	IFNAR1	IL22RA1	PDGFRB	TNFSF9
CCL24	CXCL14	IFNAR2	IL22RA2	PF4	TPO
CCL25	CXCL16	IFNB1	IL23A	PF4V1	TSLP
CCL26	CXCL2	IFNE	IL23R	PLEKHO2	VEGFA
CCL27	CXCL3	IFNG	IL24	PPBP	VEGFB
CCL28	CXCL5	IFNGR1	IL25	PPBPP1	VEGFC
CCL3	CXCL6	IFNGR2	IL26	PRL	VEGFD
CCL3L1	CXCL8	IFNK	IL2RA	PRLR	XCL1
CCL3L3	CXCL9	IFNL1	IL2RB	RELT	XCL2
CCL4	CXCR1	IFNL2	IL2RG	TGFB1	XCR1
CCL4L2	CXCR2	IFNL3	IL3	TGFB2	HIF1A
CCL5	CXCR3	IFNLR1	IL3RA	TGFB3	CEBPB
CCL7	CXCR4	IFNW1	IL4	TGFBR1	STAT1
CCL8	CXCR5	IL10	IL4R	TGFBR2	STAT3
CCR1	CXCR6	IL10RA	IL5	TNF	NOS2
CCR10	EDA	IL10RB	IL5RA	TNFRSF10A	ARG1
CCR2	EDA2R	IL11	IL6	TNFRSF10B	PTGS2
CCR3	EDAR	IL11RA	IL6R	TNFRSF10C	PTGES2
CCR4	EGF	IL12A	IL6ST	TNFRSF10D	S100A8
CCR5	EGFR	IL12B	IL7	TNFRSF11A	S100A9

Supplemental Figure 1. Semi-automated pipeline that performs batch-analyses of flow cytometry data to avoid variability intrinsic to manual analysis, and unveils full cellular diversity based on unbiased clustering. This strategy allowed the systematic identification and quantification of a variable number of cell clusters, which grouped according to the similarity of antigen expression profiles by using the bioinformatic algorithm FlowSOM.

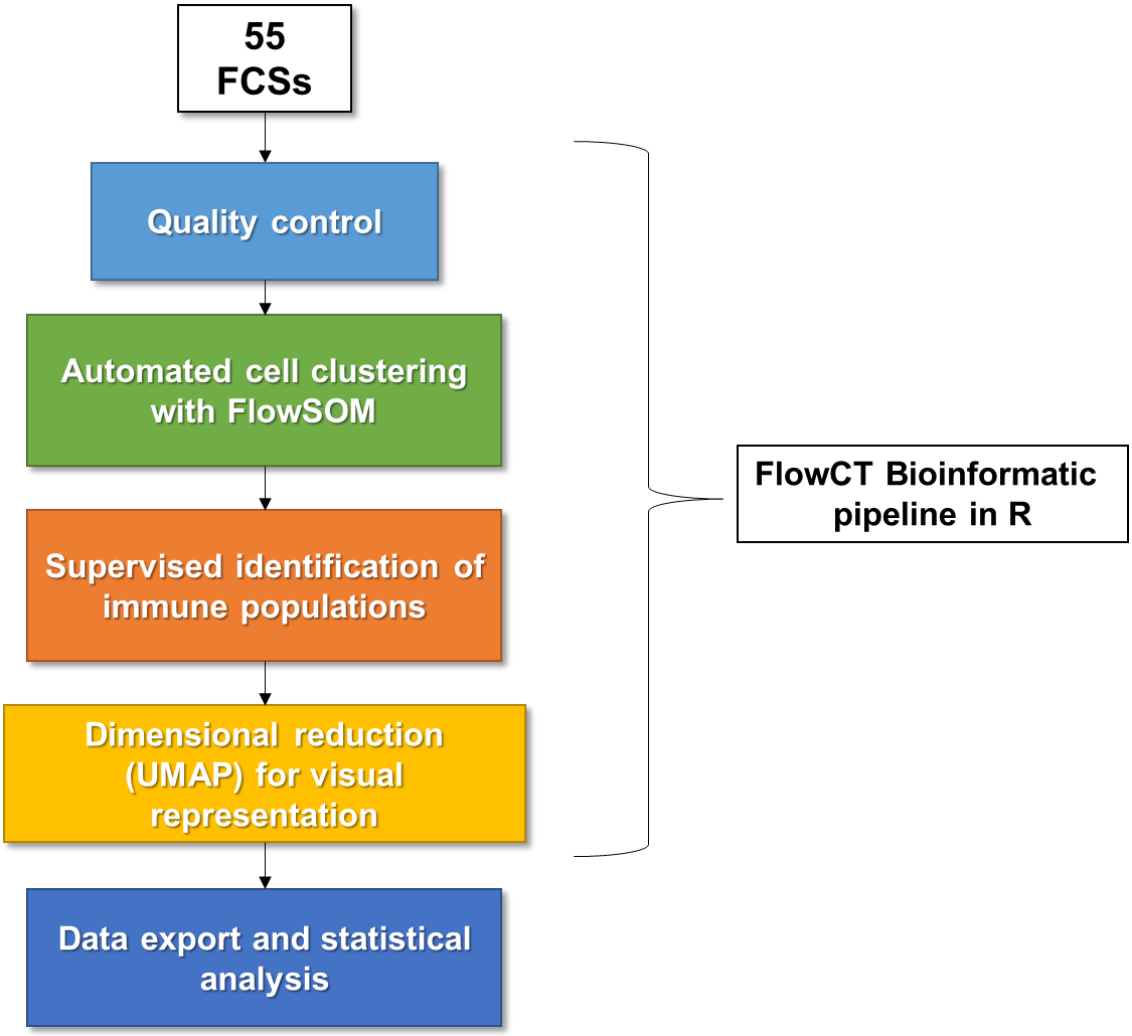

Supplemental Figure 2. Characterization of G-MDSCs based on conventional criteria. Flow cytometry analysis using the conventional gating strategy for G-MDSCs based on the expression of CD11b, CD14, CD15, CD33 and HLADR antigens. $CD11b^{+}CD14^{-}CD15^{+}CD33^{+}HLADR^{-}$ cells included a mixture of immature and mature neutrophil subsets plus eosinophils.

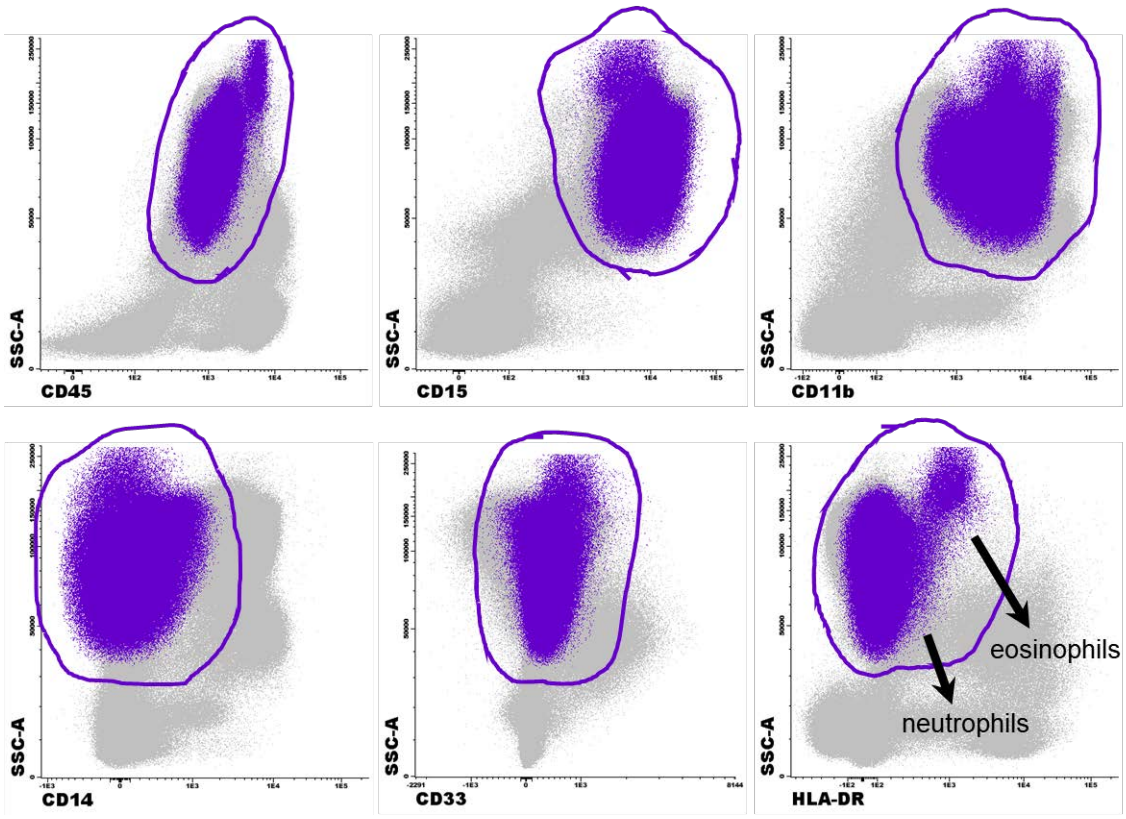

Supplemental Figure 3. Phenotypic and transcriptional profile of mature neutrophils present in matched BM and PB samples from MM patients. (A) Flow cytometry analysis of neutrophils from paired samples of BM and PB (N = 5) show no differences in the immunophenotype of BM and PB neutrophils. Boxes represent the mean and lines the standard deviation (from five independent experiments. (B) Principal component analysis of BM and PB neutrophils show that circulating mature neutrophils overlap with BM mature neutrophils. Lines represent the standard deviation and dots the median values. (C) Transcriptomic signature of mature BM and PB neutrophils show that circulating neutrophils from MM patients cluster with patient-matched BM neutrophils rather than with mature neutrophils from HA.

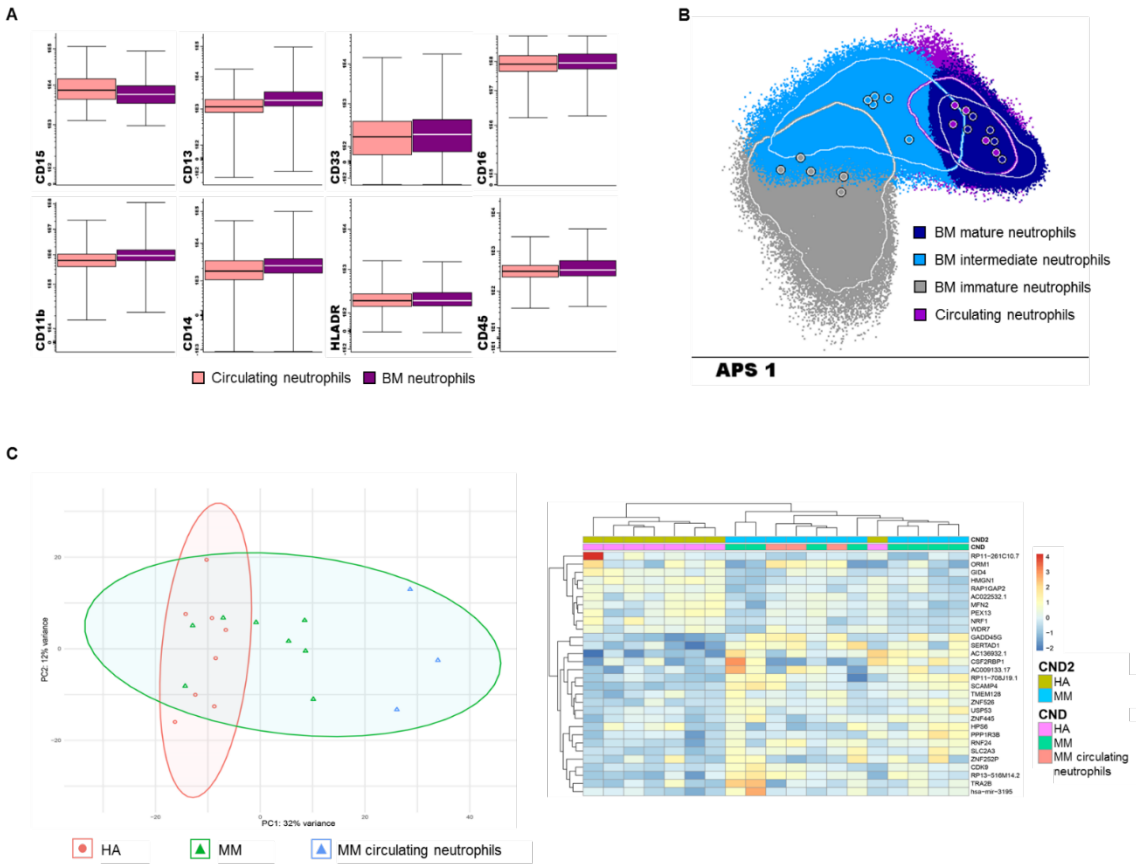

Supplemental Figure 4. Daratumumab has no long-term in vitro effect on BM granulocytes from MM patients. (A) BM samples from MM patients (N = 3) were cultured in an organoid 3D model to enable long-term treatment. **(B)** After 10-day treatment, daratumumab induced a significant depletion of tumor plasma cells. **(C)** No significant differences in the percentage of CD11b+CD14-CD15+CD33+HLADR- cells. Bar graphs represent the mean and lines the standard deviation. The statistical significance was evaluated using the t-Student test**. (D)** or any other granulocytic subsets before and after treatment. **(E)** Flow cytometry analysis of BM samples from MM patients (N = 36) before and after treatment with daratumumab show no significant differences in each granulocytic subset.

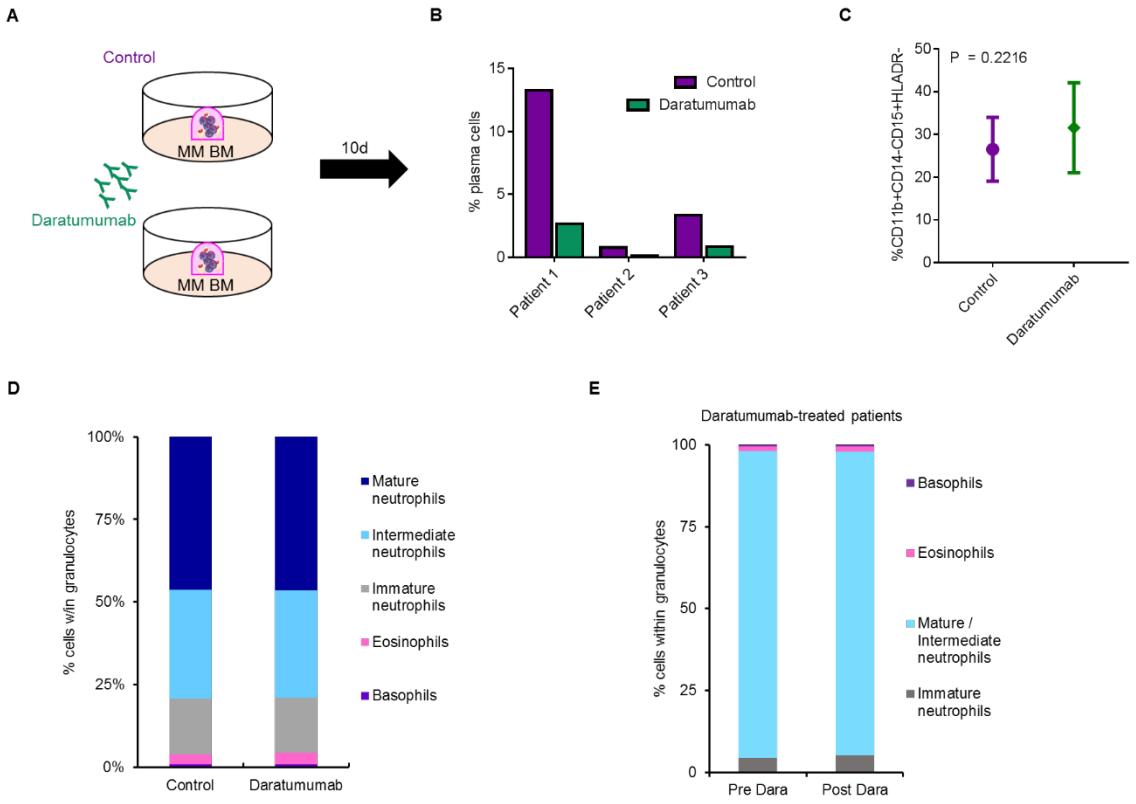

Supplemental Figure 5. (A) Correlations between granulocytic subsets and other BM populations (nucleated red blood cells –NRBCs-, T cells and tumor cells) with clinical parameters. (B) Progression-free survival according to high vs low abundance of intermediate and immature neutrophils, eosinophils and basophils). Boxes represent the mean and lines the standard deviation.

A

	Basophils	Eosinophils	Mature neutrophils	Intermediate neutrophils	Immature neutrophils	NRBCs	T cells	Tumor cells
ISS (I vs II vs III)	0.734	0.433	0.449	0.250	0.868	0.232	**0.020**	**0.010**
cytogenetic (high vs standard risk)	0.975	0.337	0.597	0.808	0.150	**0.011**	0.624	0.869
LDH (normal vs ULN)	0.193	0.315	0.246	0.824	0.632	0.541	**0.046**	0.345

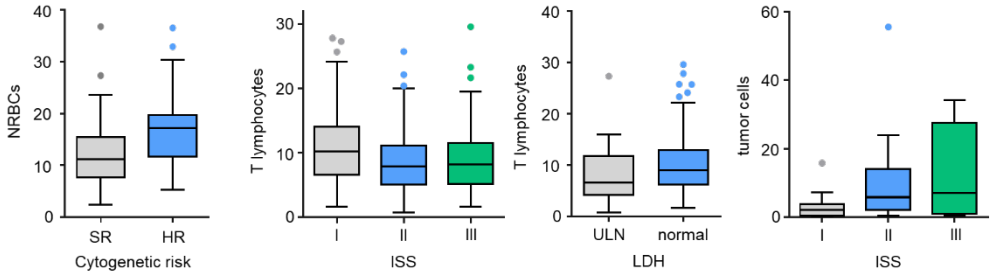

B

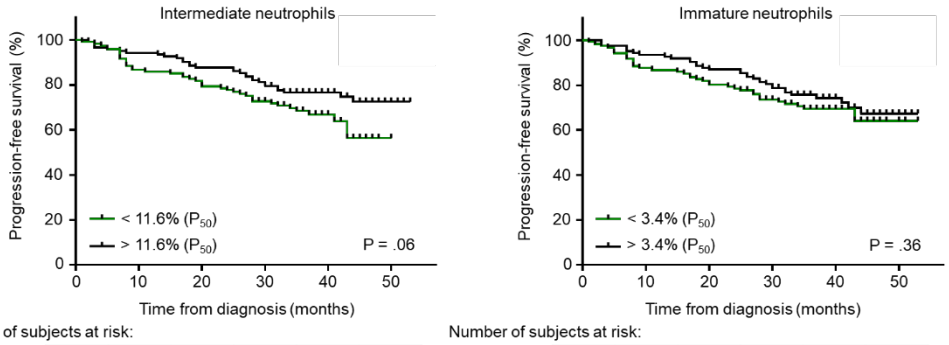

Number of subjects at risk:

Group <11.6%	131	107	99	85	25	2
Group >11.6%	136	117	109	93	49	9

Number of subjects at risk:

Group <3.4%	132	107	96	86	34	5
Group >3.4%	135	116	108	92	40	6

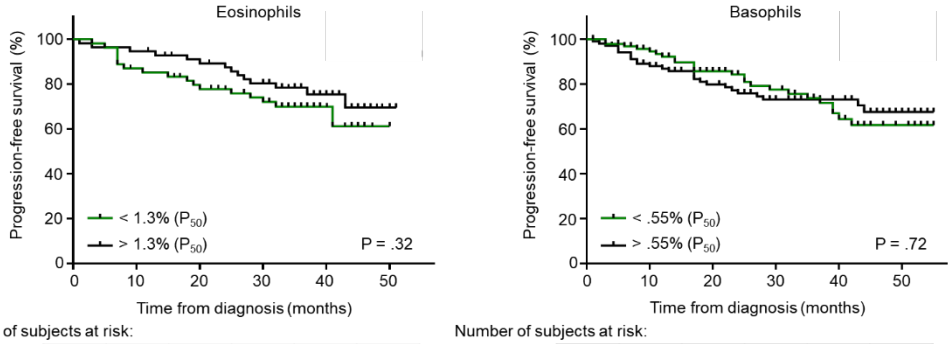

Number of subjects at risk:

Group <1.3%	131	117	104	92	27	2
Group >1.3%	136	131	123	109	44	4

Number of subjects at risk:

Group <.55%	132	110	85	65	37	6
Group >.55%	135	113	89	68	41	7

Supplemental Figure 6. (A and B) Graphical representation of 21 genes from the KEGG cytokine-cytokine receptor interaction pathway list, which displayed significantly different expression levels in immature, intermediate and mature neutrophils from healthy adults (N = 8) and multiple myeloma (MM) patients (N = 8). Patterns of gene expression were similar in HA and MM patients with the exception of a significant and progressive upregulation of VEGFA and TGFB1 and a lack of increase of CXCL1 in MM neutrophils. (C) All genes with significant differences in expression levels found in mature neutrophils from HA and MM patients.

Supplemental Figure 7. Molecular characterization of neutrophil differentiation in the BM of HA and MM patients. Unsupervised clustering of RNAseq data showed incomplete segregation between HA and MM regarding the transcriptional profile of **(A)** immature and **(B)** intermediate neutrophils.

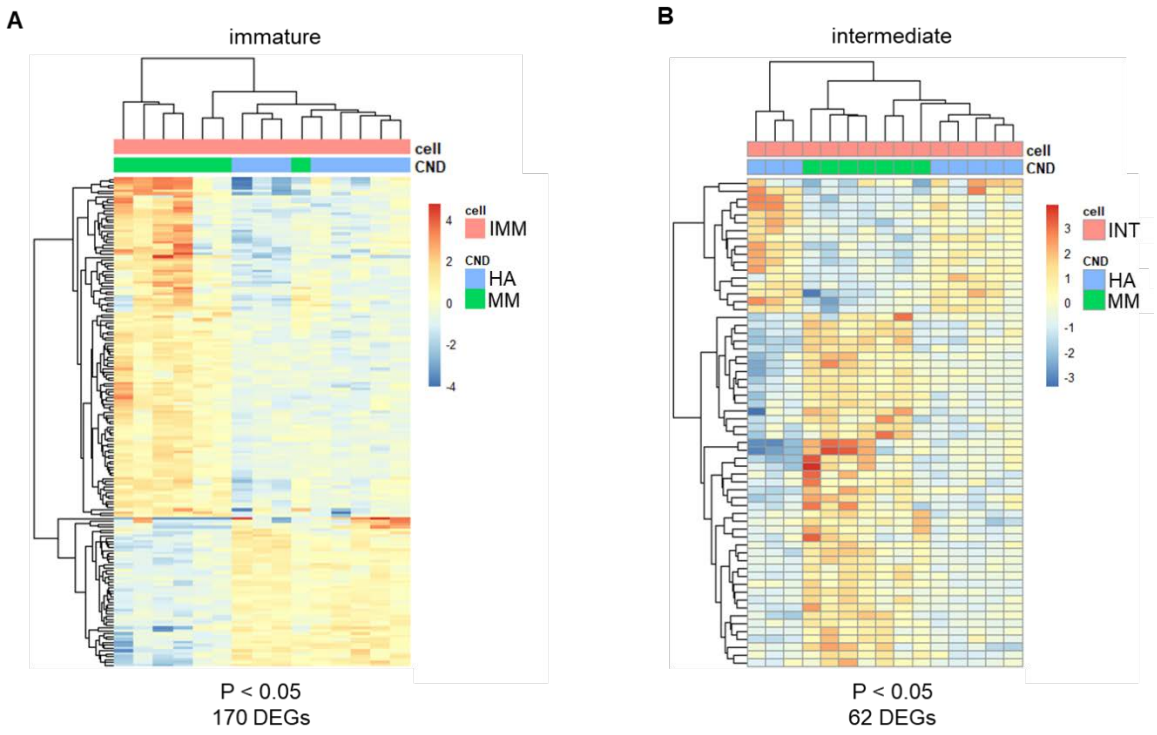

Supplemental Figure 8. Genes coding for cytokines/chemokines with significantly different expression in mesenchymal stromal cells from bone marrow aspirates of healthy adults (HA, N = 8) and multiple myeloma (MM) patients (N = 56). No differences were noted in TGF-β expression.

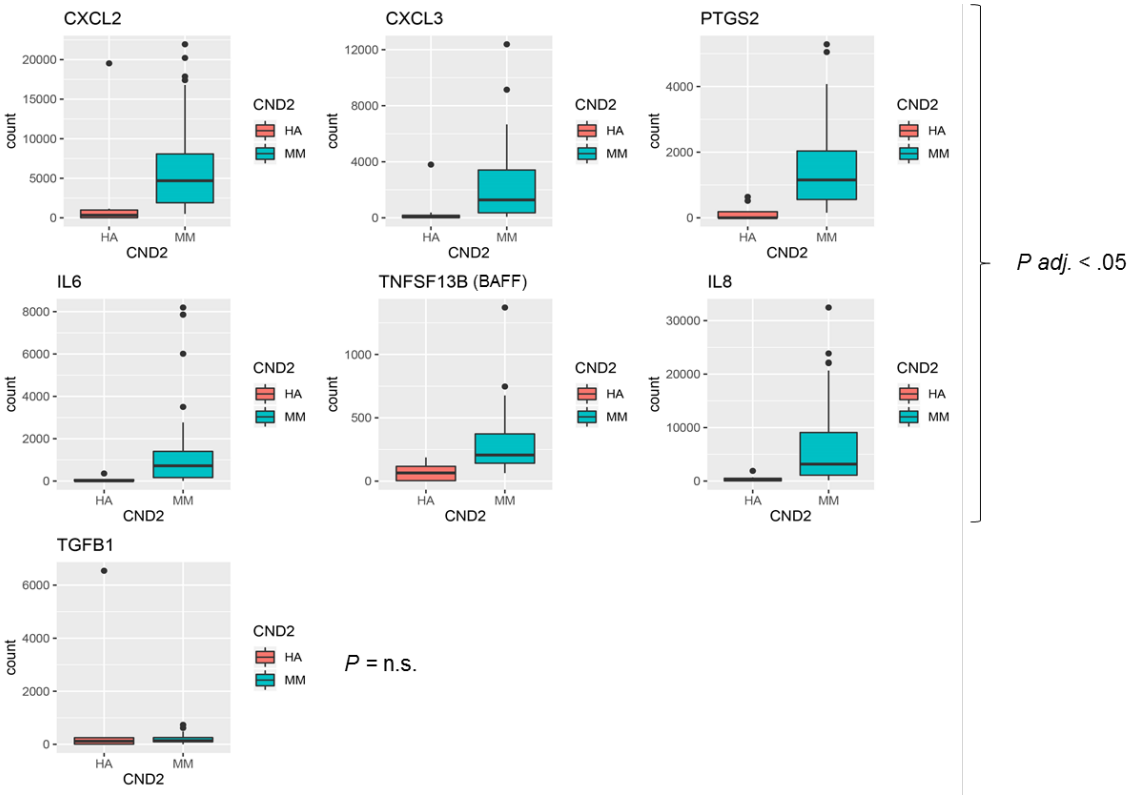

Supplemental Figure 9. The transcriptional network of mature neutrophils is epigenetically deregulated in MM. **(A)** Differential open chromatin sites (peaks) were annotated to the nearest gene based on their distance to transcription start sites (TSS). 50% of these peaks were in potential promoter regions within 3 kb of a TSS, suggesting that these gains/losses in accessibility could exert regulatory activity. **(B)** Significant correlation between gains or losses of chromatin accessibility near TSS and gene expression for each normal and tumor derived neutrophil samples based on paired ATACseq and RNAseq data. **(C)** *CD83* showed significantly higher mRNA expression in MM vs HA as well as concordant transcriptional and chromatin accessibility data. Flow cytometry data show increased protein expression in MM in accordance to molecular data. Boxes represent the mean and lines the standard deviation (from three independent experiments).

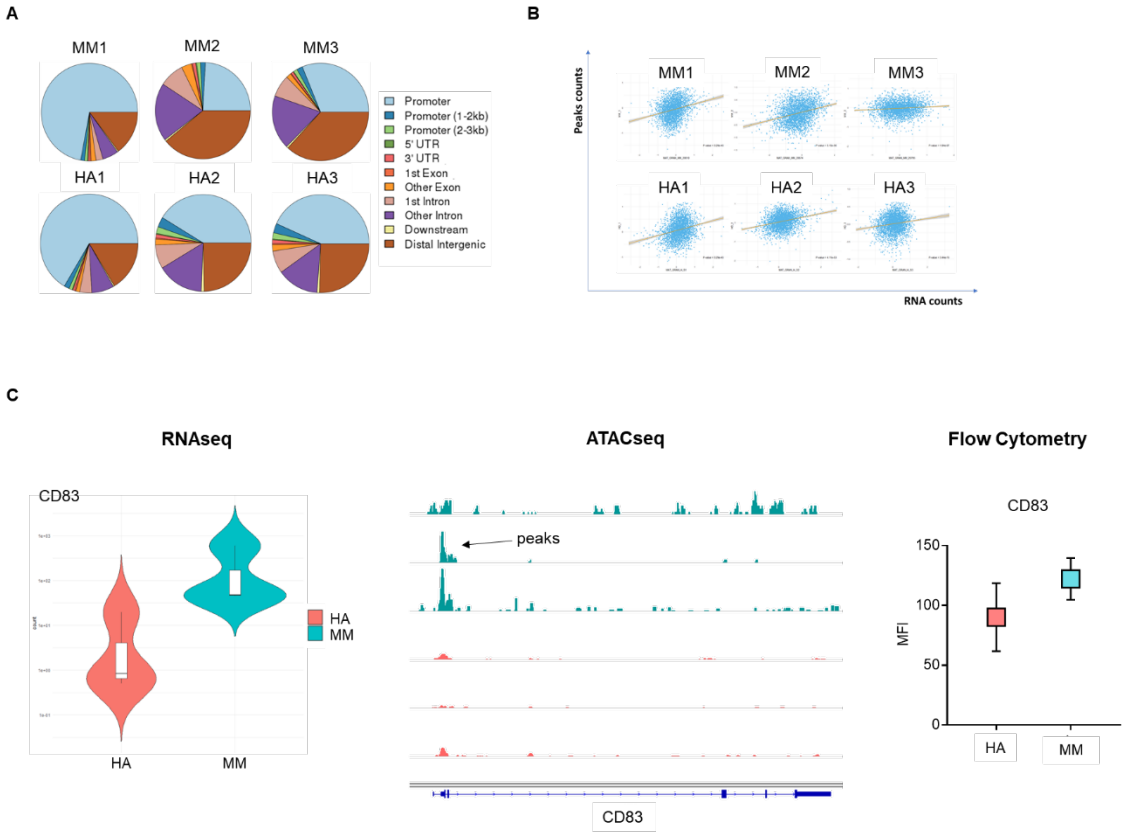

Supplemental Figure 10. Mode of action of CM-272 was confirmed by validating the induced expression of several type I IFN related genes described below.

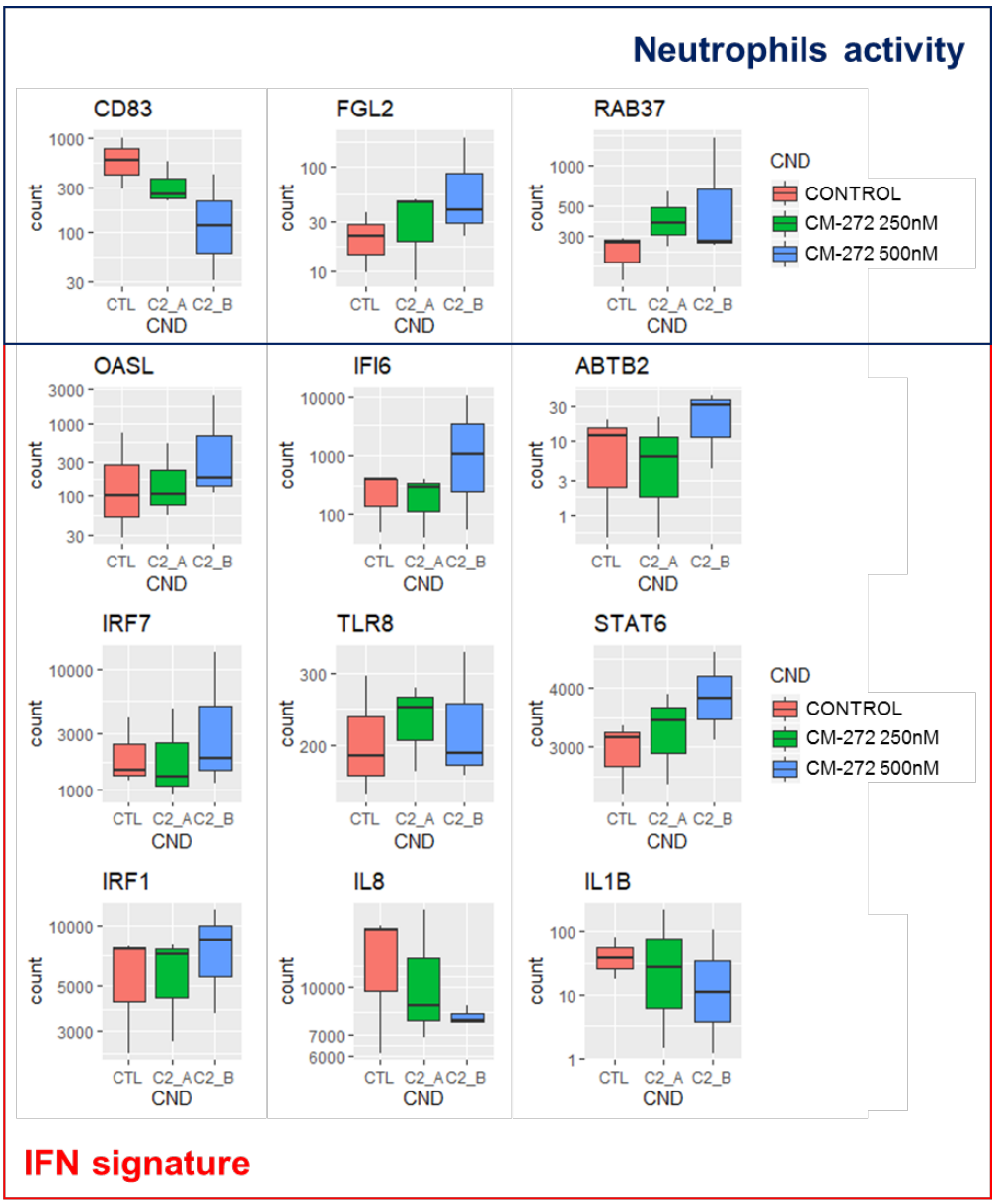

Supplemental Figure 11. Combination of CM-272 and a BCMAxCD3 bispecific antibody show that CM-272 is able to abrogate the immunosuppressive activity exerted by mature neutrophils. The combination significantly increased the activity of T cells against H929 MM cells when compared to single-agent BCMAxCD3 bispecific antibody ($P \leq .01$). Bar graphs represent the mean and lines the standard deviation (from five independent experiments).

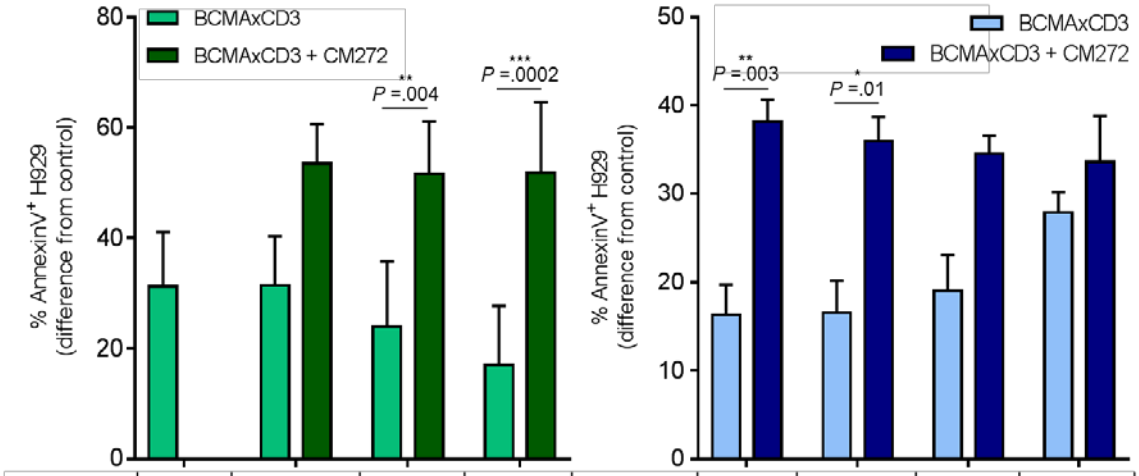

T cells	+	+	+	+	+	+	+	+
H929	+	+	+	+	+	+	+	+
Immature neutrophils	-	+	-	-	+	-	+	+
Intermediate neutrophils	-	-	+	-	+	+	-	+
Mature neutrophils	-	-	-	+	+	+	+	-